

Research Article

Comparison of Characteristics of Horseshoe Vortex at Circular and Square Piers

Subhasish Das, Rajib Das and Asis Mazumdar

¹School of Water Resources Engineering, Jadavpur University,
Kolkata-700032, West Bengal, India

Abstract: This study presents an experimental investigation on the characteristics of horseshoe vortex system within the equilibrium scour hole at circular and square pier measured by an Acoustic Doppler Velocimeter (ADV). Two tests were conducted for the approaching flow having undisturbed flow depth (= 0.125 m) greater than the pier width and the depth-averaged approaching flow velocity (= 0.247 m/s) about 68% of the critical velocity of the uniform bed sand that had a median diameter of 0.825 m. The flow measurements by the ADV were taken within the equilibrium scour hole at a circular pier of width 0.11 m. In order to have a comparative study, the ADV measurements within an equilibrium scour hole at a square pier (side facing the approaching flow) of sides equaling the width of the circular pier were also taken. The contours and distributions of the time-averaged velocities, turbulence intensities, turbulent kinetic energy and Reynolds stresses at different azimuthal planes (0° i.e., at the upstream axis of symmetry, 45° and 90°) are presented. Velocity vector plots of the flow field at azimuthal planes are used to show further flow features. The circulation of the horseshoe vortex is determined by using Stokes theorem and Forward difference technique. Bed-shear stresses are also determined from the Reynolds stress distributions. The flow characteristics of the horseshoe vortex are discussed from the point of view of the similarity with the velocity and turbulence characteristic scales.

Keywords: Circulation, flow pattern, open channel turbulent flow, scour hole, turbulence intensity, vorticity

INTRODUCTION

Prediction of the magnitude of scour at piers and abutments is a topic of importance to the field-engineers. Numerous investigations have been carried out with the purpose of predicting scour and various equations have been developed by various researchers. Review of the important experimental and field studies was given by Laursen and Toch (1956), Liu *et al.* (1961), Shen *et al.* (1969), Breusers *et al.* (1977), Jain and Fischer (1979), Raudkivi and Ettema (1983), Froehlich (1989), Melville (1992), Abed and Gasser (1993), Richardson and Richardson (1994), Barbhuiya and Dey (2004) and Khwairakpam *et al.* (2012). However, these studies primarily focus on the estimation of maximum scour depth at piers and abutments. Scour depth can be predicted more precisely if one can understand the scour mechanism from the viewpoint of the flow and turbulent characteristics of the horseshoe vortex. Melville (1975) was the pioneer to measure the turbulent flow field within a scour hole at a circular pier with the aid of the hot-film anemometer. He measured the flow field in the upstream axis of symmetry and the near-bed turbulence

intensity for the case of a flat bed, intermediate and equilibrium scour hole. He also estimated the bed-shear stresses from the measured near-bed velocities. Dey *et al.* (1995) investigated the quasi steady vortex flow field around circular piers in a clear water quasi-equilibrium scour hole. Velocity vectors were measured by a five-hole pitot sphere at different azimuthal planes 0° , 15° , 30° , 45° , 60° and 75° . Variation of circulation was presented with respect to pier Reynolds number (R_p) at 0° for all the eighteen runs. The study showed satisfactory agreement with the observations of Melville (1975). Ahmed and Rajaratnam (1998) attempted to describe the velocity distributions in the upstream axis of symmetry within a scour hole at a circular pier by using a Clauser-type defect method. Graf and Istiarto (2002) experimentally investigated the three-dimensional flow field in an established (equilibrium) scour hole. An Acoustic-Doppler Velocity Profiler (ADVP) was used to measure instantaneously the three components of the velocities in the vertical symmetry (stagnation) plane of the flow before and after the pier. The velocities, turbulence intensities, Reynolds stresses, bed-shear stresses and vorticity of the flow field were calculated in different

Corresponding Author: Subhasish Das, School of Water Resources Engineering, Jadavpur University, Kolkata-700032, West Bengal, India, Tel.: +91 33 2414-6161, Fax: +91 33 2414-6886

This work is licensed under a Creative Commons Attribution 4.0 International License (URL: <http://creativecommons.org/licenses/by/4.0/>).

azimuthal planes within the equilibrium scour hole at a circular pier. Results of the study showed that a vortex-system was established in the front and a trailing wake-vortex system of strong turbulence was formed in the rear of the pier. Muzzammil and Gangadhariah (2003) investigated experimentally that the primary horseshoe vortex formed in front of a cylindrical pier which is the prime agent responsible for scour during the entire process of scouring. An expression for the maximum equilibrium scour depth was also developed from the vortex velocity distribution inside scour hole. The resulting scour prediction equation was found to give better results compared to the results of well-known predictor models when applied to model scour data. Dey and Raikar (2007) presented the outcome of an experimental study on the turbulent horseshoe vortex flow within the developing intermediate stages [having scour depth (d_s) of 0.25, 0.5 and 0.75 times the equilibrium scour depth (d_{se})] and equilibrium scour holes at cylindrical and square piers measured by an Acoustic Doppler Velocimeter (ADV). The contours of the time-averaged velocities, turbulence intensities and Reynolds stresses at different azimuthal planes 0° , 45° and 90° were presented. It was observed that the flow and turbulence intensities in the horseshoe vortex flow in a developing scour hole are reasonably similar.

The present study reports the difference between the flow and turbulence characteristics of horseshoe vortex at equilibrium scour condition at circular and square pier of same width. However, the flow zone downstream the pier is beyond the scope of the study, as downstream (beyond 90°) the pier, the horseshoe vortex attenuates considerably being insignificant.

EXPERIMENTAL SETUP AND PROCEDURE

In the present study investigation of scour depth and velocity measurement by ADV around circular and square pier (side facing the approaching flow) have been carried out. The experimental setup and conditions of the study were described in details with the help of the schematic diagrams as shown in Fig. 1 and 2. All the experiments were conducted in the Fluvial Hydraulics Laboratory of the School of Water Resources Engineering in Jadavpur University, Kolkata, India.

The experiments were carried out in a recirculating flume 11 m long, 0.81 m wide and 0.60 m deep. The working section of the flume was filled with sand to a uniform thickness of 0.20 m, length of the sand bed 3 m and width 0.81 m. The sand bed was located 2.9 m upstream from the flume inlet. The recirculating flow system was served by a 10 hp variable speed centrifugal pump which was located at the upstream end of the tilting flume. The rpm of the pump was 1450; power 7.5 kW, maximum discharge was 25.5 l/s. The water discharge was measured by a flow meter connected to the upstream pipe at the inlet of the flume. Water flows through a 0.2 m diameter pipe line which runs directly into the flume.

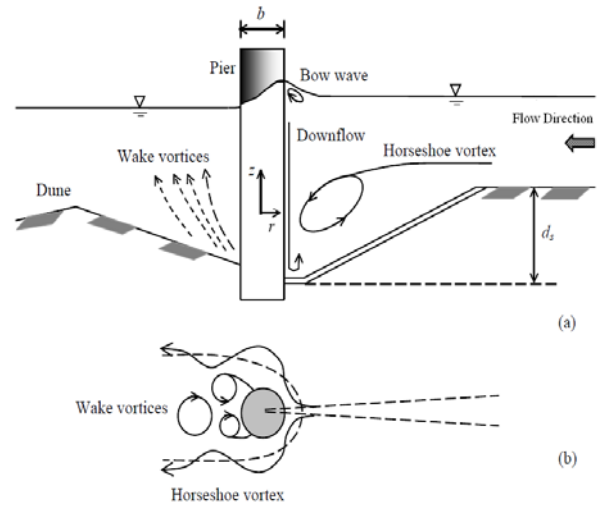


Fig. 1: Flow structure at cylindrical pier (a) elevation and (b) plan

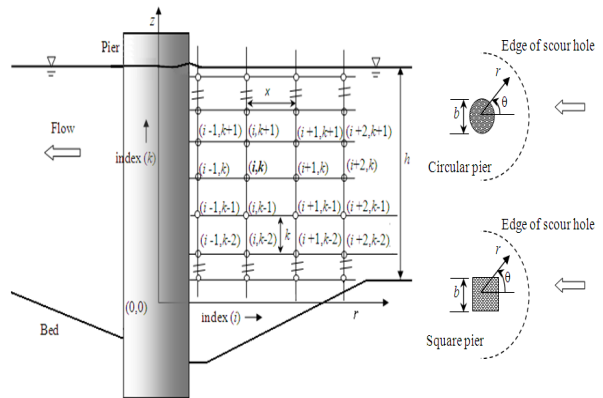


Fig. 2: Schematic diagram showing the coordinate system and grid points for ADV measurements

A movable trolley with a point gauge attached to it was positioned on the flume. A vertical scale was fixed with the point gauge to measure the water level, initial bed level and scour depth. Piers were placed in the middle of the working section of the flume. During the experiment it was kept in mind that the width of the experimental flume is more than seven times of the pier width to avoid the wall friction factor. The minimum value of the ratio between flume width and pier width is 6.25, proposed by Raudkivi and Ettema (1983) that could be used without a measurable effect from the side walls on the local scour at the pier. Both the experiments in the present study were carried out using one bed material. The bed material size was: d_{50} (= 0.825 mm), d_{16} (= 0.5 mm), d_{84} (= 1.62 mm) and d_{90} (= 1.78 mm) were measured from the sieve analysis test using a vibrating shaker. Geometric standard deviation of sediment size $\sigma_g = (d_{84}/d_{16})^{0.5}$ was 1.8. Relative density of the sand (s) was measured as 2.582. The

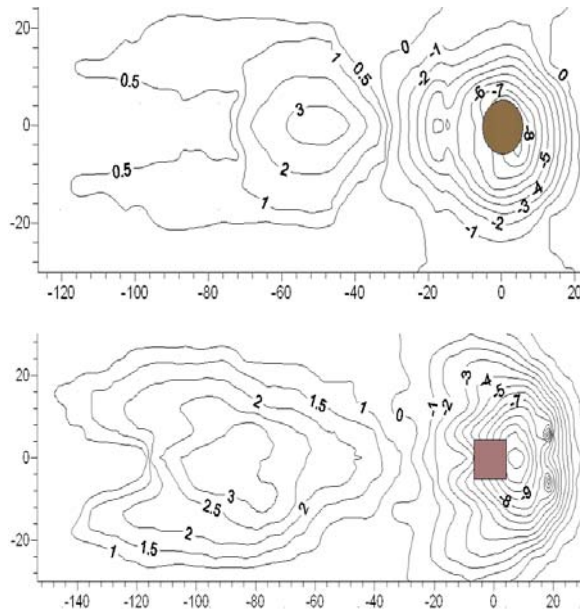


Fig. 3: Scour contours for (a) circular pier and (b) square pier

average bed shear stress was 0.39 Pa. The angle of repose (ϕ) and critical bed shear stress (τ_c) were estimated as 36° and 0.40 Pa respectively.

The flow depth in the flume was adjusted by a tailgate. The approaching flow depth (h) was maintained as 0.125 m by operating the tailgate. The bed slope ($= : 2400$) was kept constant for both the experiments. Both the experiments were conducted for the approaching flow having undisturbed flow depth where the ratio between the approach flow depth (h) and pier width ($b = 0.11$ m) was 1.14 i.e., $0.6 < h/b < 1.6$. Then the equation of The depth-averaged approaching flow velocity (U) was set as 0.247 m/s, which is about 68% of the critical velocity (u_c) of the uniform sand bed considering side-wall effect to satisfy the clear water condition i.e., the present research considered only clear water approach flow conditions described by a threshold/critical Froude number of $0.67 \leq F_r = U/u_c \leq 0.99$ (Dey and Raikar, 2007; Oliveto and Hager, 2002). The depth averaged approaching flow velocity was found out from the measured vertical profile of the approaching flow velocity at 2 m upstream of the pier where the presence of the pier did not affect the approaching flow. Froude number (F_r), flow Reynolds number (R_e) and pier Reynolds number (R_p) for both the experiments were calculated as 0.223, 2.4×10^4 and 2.8×10^4 respectively.

When negligible (1 mm or less) difference of scour depth was observed at an interval of 2 h after 72 h, it was considered that an equilibrium stage of the scour hole was attained. However, total duration of each

experiment was 80 h that was adequate for achieving the equilibrium scour (Dey and Raikar, 2007). After the run was ended, the maximum equilibrium scour depths were observed at the upstream base of the piers. Then the maximum scour depth at an equilibrium state was carefully measured by a Vernier point gauge. The contour lines of the scour holes at the circular and square piers were plotted by Golden software Surfer 8 version as shown in Fig. 3. After carefully draining out the water from the scour hole, when the bed was plausibly dry, a synthetic resin mixed with water (1:3 by volume) was sprayed uniformly over the scoured bed to stabilize and freeze it. The sand bed was sufficiently saturated with the resin when it was left to set for a period of 48 h. Having dried further up to 72 h, the scoured bed profile became rock-hard, facilitating the ADV measurements.

A cylindrical polar coordinate system was used to represent the flow and turbulence fields for both the experiments. A three-beam 5 cm down-looking ADV (16 MHz MicroADV Lab Model), manufactured by Sontek was used to measure the instantaneous three-dimensional velocity components. A sampling rate of 50 Hz and cylindrical sampling volume 0.09 cm^3 having 1-5 mm sampling height were set for the measurements. Sampling heights 5 and 1-2 mm were used for measurement of velocity components above and within the interfacial sub-layer (when velocity component decreases rapidly), respectively. A sampling duration of 120-300 s was considered ensuring a statistically time-independent averaged velocity. The sampling durations were relatively long near the bed. The ADV reading were taken along several vertical lines at different azimuthal plane. The lowest horizontal resolution of the ADV measurements was 0.9 cm. Vector plots representing characteristic of the flow field do not show all experimental data at the lowest resolution in order to avoid overlapping or congested plots. The measurement by ADV probe was not possible below in the zone 4.5 mm above the sand bed, because the ADV needs a measuring volume of 0.09 cm^3 . The output data from the ADV were filtered using a software WinADV32 -version 2.027 developed by Tony L. Wahl. During the filtering of ADV data, the minimum Signal-to-Noise Ratio (SNR) and the minimum correlation parameter were maintained 15 and 70%, respectively.

ANALYSES OF FLOW AND TURBULENT FIELDS

In cylindrical polar coordinates as shown in Fig. 2, the time-averaged velocity components in (θ, r, z) are represented by (u, v, w), whose corresponding

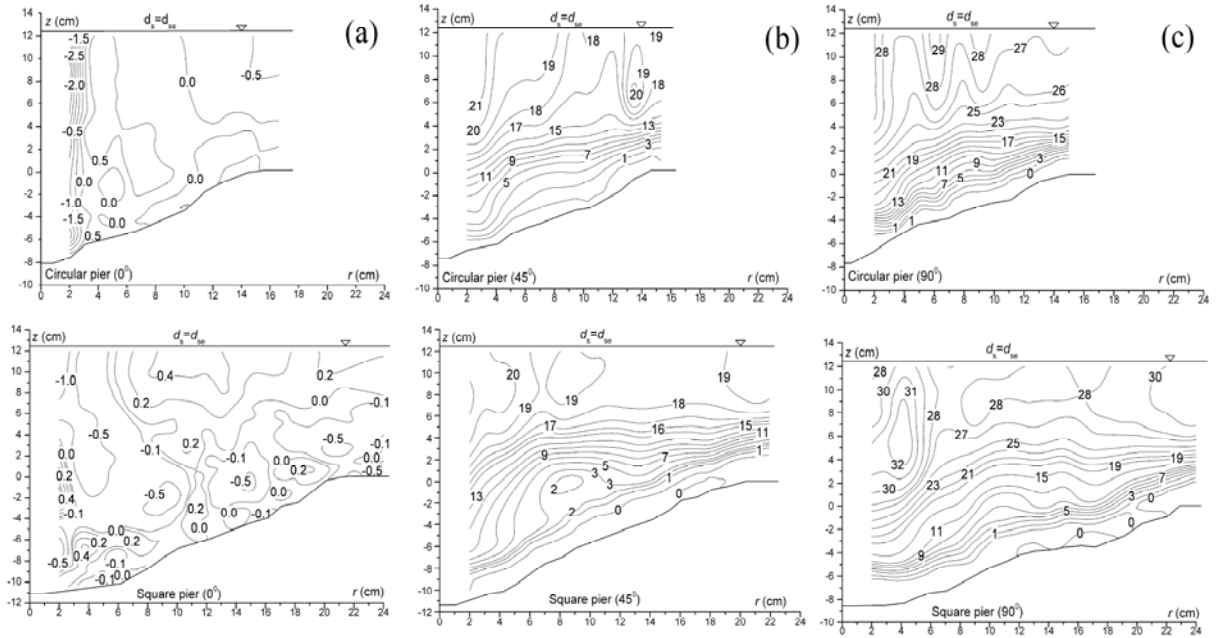


Fig. 4: Contour of time-averaged tangential velocity u (in cm/s) at azimuthal planes (a) $\theta = 0^\circ$, (b) $\theta = 45^\circ$ and (c) $\theta = 90^\circ$

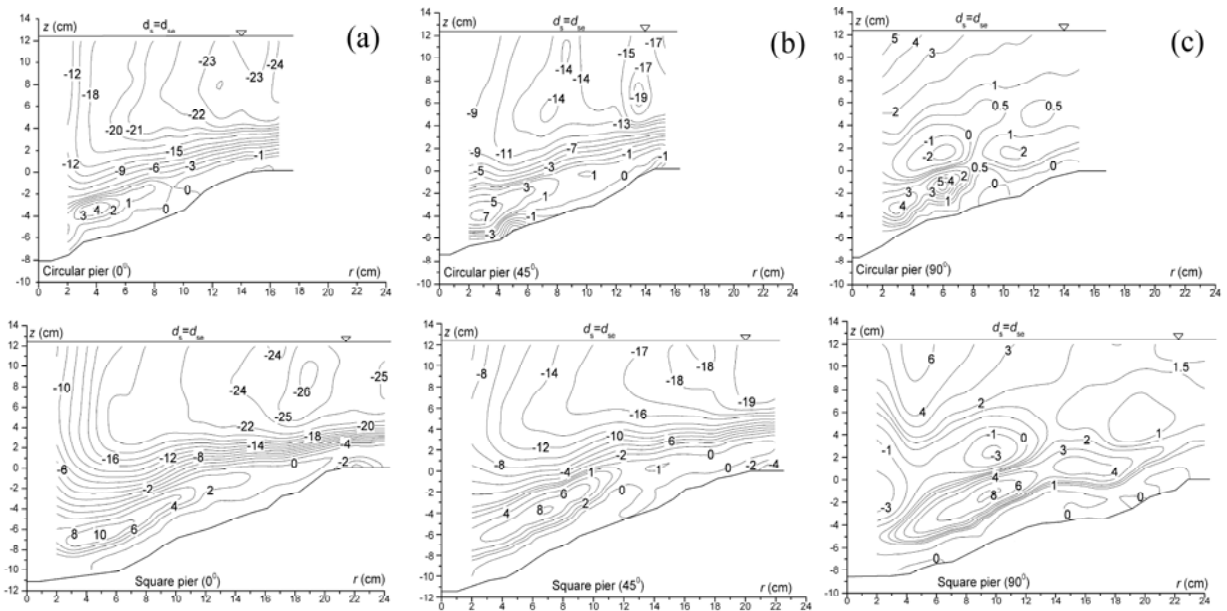


Fig. 5: Contour of time-averaged radial velocity v (in cm/s) at azimuthal planes (a) $\theta = 0^\circ$, (b) $\theta = 45^\circ$ and (c) $\theta = 90^\circ$

fluctuations are (u', v', w') . The positive directions of u , v and w are anticlockwise, outward and upward, respectively. The velocity and turbulence fields are plotted in an rz plane at different azimuthal angles ($= 0^\circ, 45^\circ$ and 90°). The resolutions in the ordinate are taken larger than those in the abscissa to have a clear representation of the flow field within the equilibrium scour holes which are smaller in dimension. It is important to point out that the outer radius of the ADV sensor was 2.5 cm having three receiving transducers

mounted on short arms around the transmitting transducer at 120° azimuth intervals, which made it possible to measure the flow as close as 2 cm from the pier boundary.

Flow fields: The contours (plotted by OriginLab Software) of time-averaged tangential velocity u for circular and square piers at different azimuthal planes ($0^\circ, 45^\circ$ and 90°) are shown in Fig. 4a to c, which represent the characteristics of the passage of the flow by the side of the pier. Importantly, it drives the

horseshoe vortex toward the pier downstream. At 0° (i.e., at the upstream axis of symmetry) the tangential velocity u , which is essentially zero, is negligible as was detected by the ADV. However, it becomes finite and increases with increase in azimuthal angle θ . For example, the magnitude of u at 90° is 1.3-1.6 times greater than that of u at 45° at the corresponding locations. The passage of the downflow flux by the side of the pier results in a considerable enhancement of u near the pier and thus u decreases with increase in radial distance r from the pier and remains almost constant over the flat bed. The magnitude of u increases with increase in z and the vertical gradient of u (that is $\partial u/\partial z$) within the scour hole (that is $z \leq 0$) is more than that above the scour hole (that is $z > 0$). On the other hand, for a square pier, the magnitudes of u are smaller than those of a circular pier at the corresponding locations at equilibrium scour hole, as the size of the scour hole at a square pier is larger than that at a circular pier.

The contours of the time-averaged radial velocity v at different azimuthal planes (0° , 45° and 90°) for equilibrium scour holes at circular and square piers are shown in Fig. 5a to c. At 0° , the separation of the approaching flow is evident just beneath the edge of the scour hole forming a reversal flow inside the scour hole ($z \leq 0$). Thus, radial velocity v changes direction on either side of the contour line of $v = 0$, which falls approximately at the depths that are 0.4-0.45 times the local depth of the scour hole below the original bed level. It confirms that in the pier upstream, a strong horseshoe vortex exists inside the scour hole. The variations of v in the zones $z \leq 0$ and $z > 0$ are not similar. The magnitude of v becomes positive (away from the pier) near the bed as the flow returns from the base of the pier resulting in a reversed flow along the sloping bed of the scour hole. The magnitude of the maximum reversed velocity that occurs near the base of the pier is approximately $0.3U$. In $z > 0$, v is negative (toward the pier) and unidirectional whose variation along z being relatively less is almost logarithmic due to the influence of the approaching flow, becoming maximum near the free surface. On the upstream flat bed, v remains essentially logarithmic and decreases upon entering the scour hole due to the exposure of larger flow area. Then, it progressively diminishes toward the pier. This is due to the existence of the pier (vertical solid boundary) and an increase of the scour depth toward the pier. At 45° , though the overall distribution of v is almost similar (having magnitude of v smaller than that at the corresponding locations of the flow zone at a circular pier at 0°), the line of separation is shallower (approximately 0.72-0.77 times the local scour depth from the original bed level) as compared to that at 0° .

The reducing nature of v with increase in θ is obvious from 0° to 90° as a result of horseshoe vortex reduction, whereas at 0° the distribution of v is

strongest. Dey *et al.* (1995) and Dey (1995) showed that the horseshoe vortex detaches from the pier at 75° , which was the reason to detect the flow at 90° being out of phase from those at 0° and 45° . In spite of that, the overall flow feature at 90° can be summarized as v acts toward the pier within the scour hole ($z \leq 0$) (though there exists a thin zone of reversed flow close to the bed) and above the scour hole ($z > 0$) the flow deflects outwards by the side of the pier. On the other hand at 0° and 45° , the distributions of v at a square pier are similar to those at a circular pier; it is different at 90° , because the flow separation takes place at 45° from the sharp edge of the square pier. This is the reason why there exists lower v near the pier. However, at 0° and 45° , the nature of flow at a square pier is similar to that at a circular pier having magnitude of v greater than that at the corresponding locations of the flow zone at a circular pier.

Figure 6a to c show the contours of the time-averaged vertical velocity w at different azimuthal planes (0° , 45° and 90°) for equilibrium scour holes at circular and square piers. From an observation of the contours of vertical velocity w at 0° , the separation of the approaching flow below the edge of the scour hole is evident (as it was in v contours) from the reversal nature of w near the scoured bed. While w near the scoured bed is directed upward (that is positive), the distribution of w in the majority of the flow zone is downward (that is negative). The magnitude of w increases in the downward direction from the free surface indicating that there is an existence of a downward negative pressure gradient. There is a core of the maximum w (encircled by the higher magnitudes of w) that occurs near the pier approximately at a depth of 0.3 times the local scour depth below the original bed level and then it decreases toward the base of the scour hole. This confirms the existence of a strong downflow (along the upstream face of the pier) that turns near the base of the pier forming a vortical flow within the scour hole.

The maximum magnitude of w at $\theta = 0^\circ$ measured was $0.65U$ at $z = -0.005$ m for the circular pier and $0.7U$ at $z = -0.021$ m for the square pier. This magnitude for circular pier is slightly higher than Istiarto and Graf (2001) and Dey and Raikar (2007) $0.6U$, while it is slightly lower than that of Melville (1975) $0.8U$, because the ADV measurement at the boundary of the pier was not possible. The magnitude of w decreases with increase in θ . This shows the attenuation of the horseshoe vortex toward the downstream. For instance, the maximum magnitudes of downflow for circular pier at 45° and 90° are 0.73 and 0.44 times and for square pier at 45° and 90° are 0.8 and 0.53 times that at 0° . On the other hand, for a square pier, the nature of flow is similar to that of a circular pier having magnitude of downflow greater than that at the corresponding locations of the flow zone at a circular pier by approximately 15-20%.

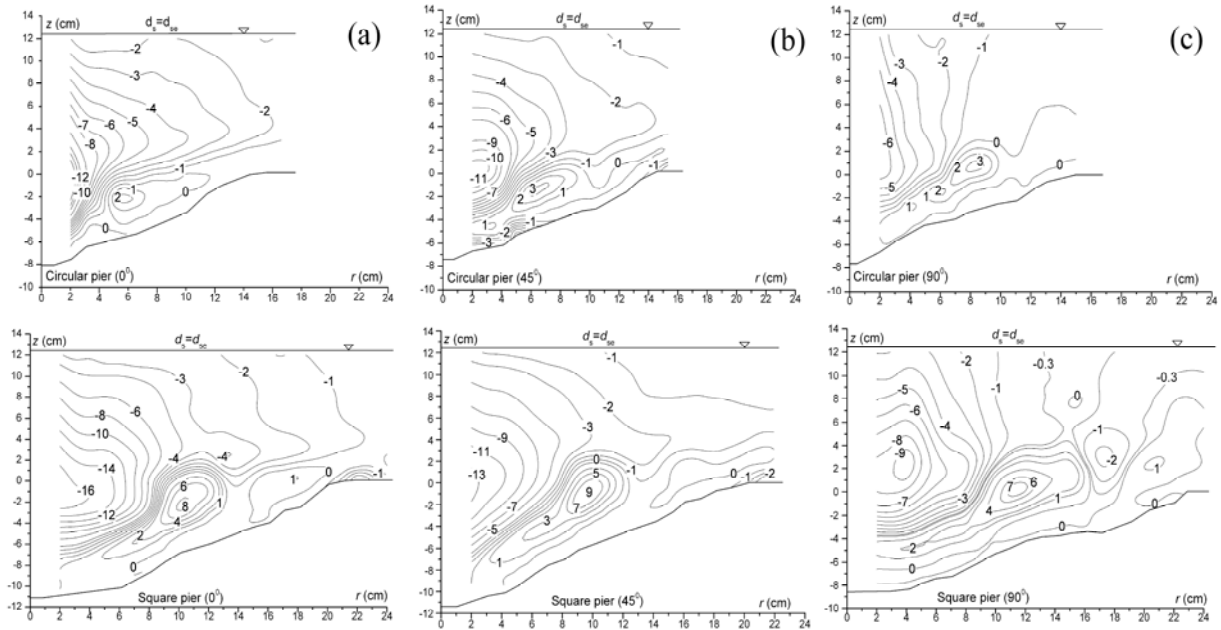


Fig. 6: Contour of time-averaged vertical velocity w (in cm/s) at azimuthal planes (a) $\theta = 0^\circ$, (b) $\theta = 45^\circ$ and (c) $\theta = 90^\circ$

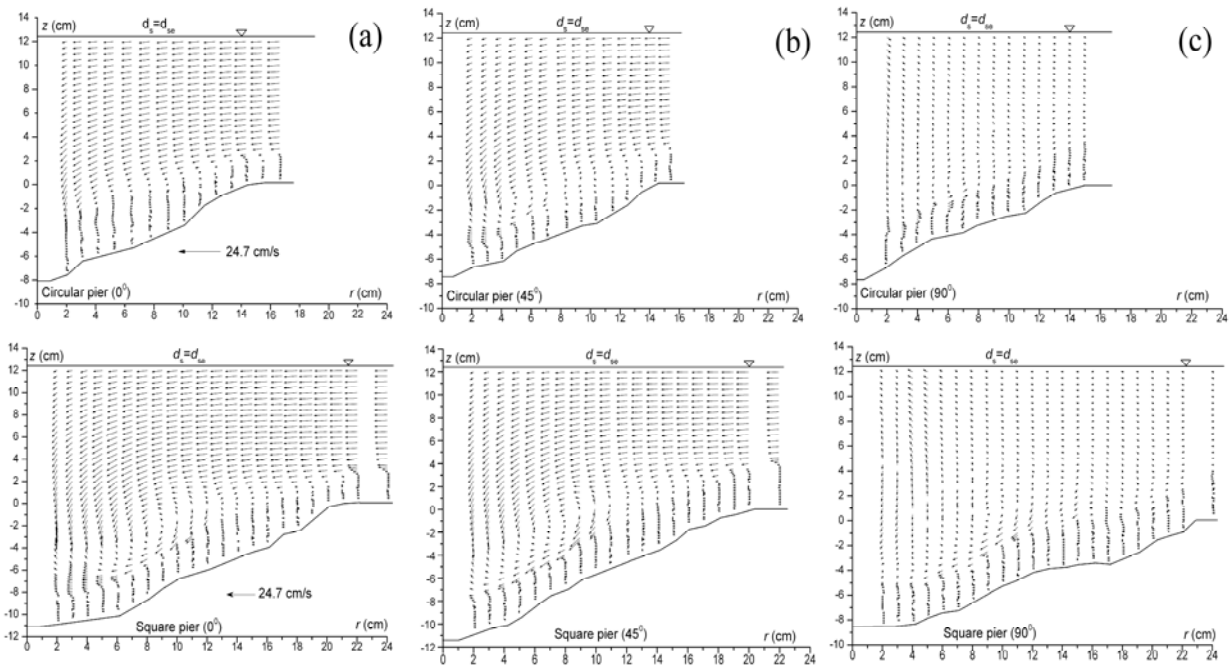


Fig. 7: Velocity vectors at azimuthal planes (a) $\theta = 0^\circ$, (b) $\theta = 45^\circ$ and (c) $\theta = 90^\circ$

The time-averaged velocity vectors, whose magnitude and direction are and, respectively, at different azimuthal planes (0° , 45° and 90°) for the equilibrium scour hole are shown in Fig. 7a to c. The vector plots at 0° and 45° exhibit the characteristics of the horseshoe vortex along with the downflow along the upstream face of the pier. The horseshoe vortex is a forced vortex type of flow, because the whirl velocity increases in the outward direction from the vortex

center. The shape of the vortex is elliptical in cross section with its major axis approximately bisecting the angle made by the slope of the scour hole with the horizontal. It is clear that the height (length of the minor axis) of the elliptical vortex at 0° is larger than that at 45° . The vortical flow is strongest at 0° , while it decreases with an increase in θ . Above the scour hole ($z > 0$), the flow is horizontal and towards the pier, but it is downward close to the pier. At 90° , the vortical flow

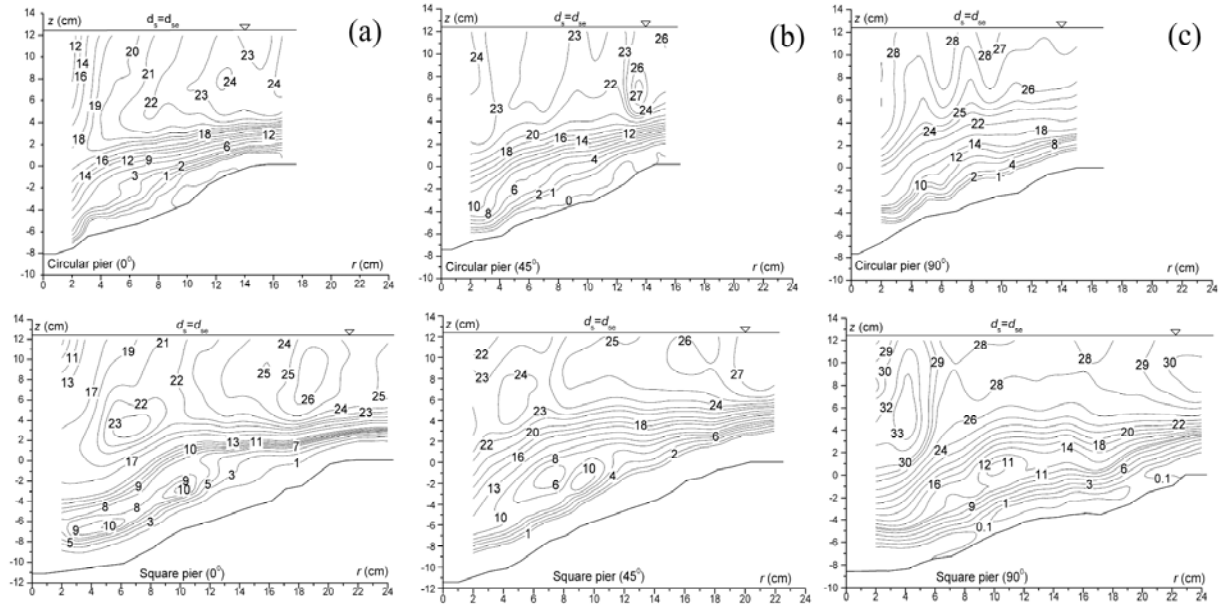


Fig. 8: Contour of time-averaged absolute velocity V (in cm/s) at azimuthal planes (a) $\theta = 0^\circ$, (b) $\theta = 45^\circ$ and (c) $\theta = 90^\circ$

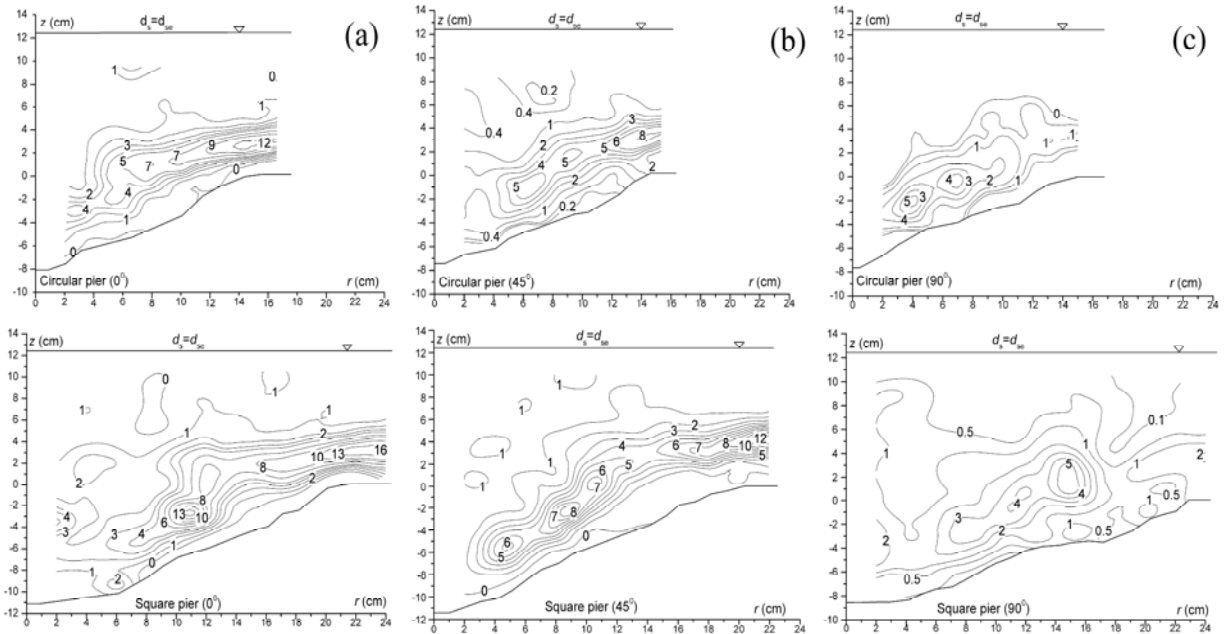


Fig. 9: Contours of vorticity ω (in s^{-1}) at azimuthal planes (a) $\theta = 0^\circ$, (b) $\theta = 45^\circ$ and (c) $\theta = 90^\circ$

is not distinct due to the separated flow. However, a close inspection of the vector field at 90° reveals that a weak vortical flow exists near the scoured bed.

Figure 8a to c indicate the time-averaged absolute velocity contours at different azimuthal planes (0° , 45° and 90°) for the equilibrium scour hole. It displays the exclusive vortical flow at 0° due to the absence of tangential velocity u . On the other hand, at 90° , tangential velocity u is a predominant flow feature. At 45° , the diminishing nature of the horseshoe vortex with θ is exhibited. The contours lines of V are

concentrated near the scoured bed, indicating a region of rapid change of the magnitude of velocity. At 90° , the magnitudes of v and w are negligible close to the pier as the side of the pier is parallel to the flow and the flow separation takes place at 45° from the sharp edge of the pier, resulting in the lower magnitude of V near the pier.

Vorticity and circulation: Figure 9a to c show the vorticity ω ($= \partial v / \partial z - \partial w / \partial r$) contours at different azimuthal planes (0° , 45° and 90°) at equilibrium scour

Table 1: Circulations for different azimuthal angles at equilibrium scour condition

Pier type	Circulation (m ² /s)		
	$\theta = 0^\circ$	$\theta = 45^\circ$	$\theta = 90^\circ$
Circular	2.785×10^{-2}	2.123×10^{-2}	0.668×10^{-2}
Square	5.553×10^{-2}	3.798×10^{-2}	1.729×10^{-2}

hole. The vorticity contours are computed from the contours of v and w given in Fig. 5 and 6. The left hand convention that is positive in anticlockwise direction is adopted to define the vorticity. The concentration of the vorticity inside the scour hole is revealed in Fig. 9a to c. From the examination of the vector plots and the vorticity contours, it confirms that it is a forced vortex. The higher magnitude of vorticity near the center of the horseshoe vortex signifies the vortex core. The size of the vortex core decreases with an increase in θ , becoming smallest at 90° . The vorticity is considerably weak at 90° . The circulation Γ of the horseshoe vortex is computed from the vorticity contours as shown in Fig. 9a to c by using the Stokes theorem. It is:

$$\Gamma = \oint_C \vec{V} \cdot d\vec{s} = \iint_A \omega \cdot dA \quad (1)$$

where, \vec{V} is the velocity vector; $d\vec{s}$ is the differential displacement vector over a closed curve and A is an area enclosed between successive vorticity contours.

Table 1 provides the circulations Γ calculated for different azimuthal planes. The magnitude of Γ decreases with an increase in θ . The magnitudes of Γ at

45° and 90° are 0.68–0.76 and 0.24–0.31 times Γ at 0° , respectively, at equilibrium scour hole. The results are in conformity with Dey and Raikar (2007).

Turbulence fields: The contours of the turbulence intensities, where u' is the fluctuation of u , v' is the fluctuation of v and w' is the fluctuation of w at different azimuthal planes (0° , 45° and 90°) for the equilibrium scour hole are shown in Fig. 10a to c, 11a to c and 12a to c, respectively. The turbulence intensities are the Root-Mean-Square (RMS) values of the velocity fluctuations. From Fig. 10a to c, 11a to c and 12a to c, it is revealed that the distributions of u^+ , v^+ and w^+ are almost similar. A core of high turbulence intensity occurs inside the scour hole as a result of flow separation and then the turbulence intensities decrease with an increase in r and z . There is trivial change in the distribution patterns of u^+ , v^+ and w^+ with θ . Except for horizontal plane (that is the θr plane), the turbulence characteristics are non-isotropic, because the mean values (and standard deviation values) of the ratios of u^+/v^+ , v^+/w^+ and w^+/u^+ are 0.987 (0.238), 2.428 (1.657) and 0.608 (0.304), respectively. The contours of the turbulent kinetic energy $k \left[= 0.5(u'^2 + v'^2 + w'^2) \right]$ are exhibited in Fig. 13a to c to illustrate the distributions of k that are similar to those of turbulence intensities.

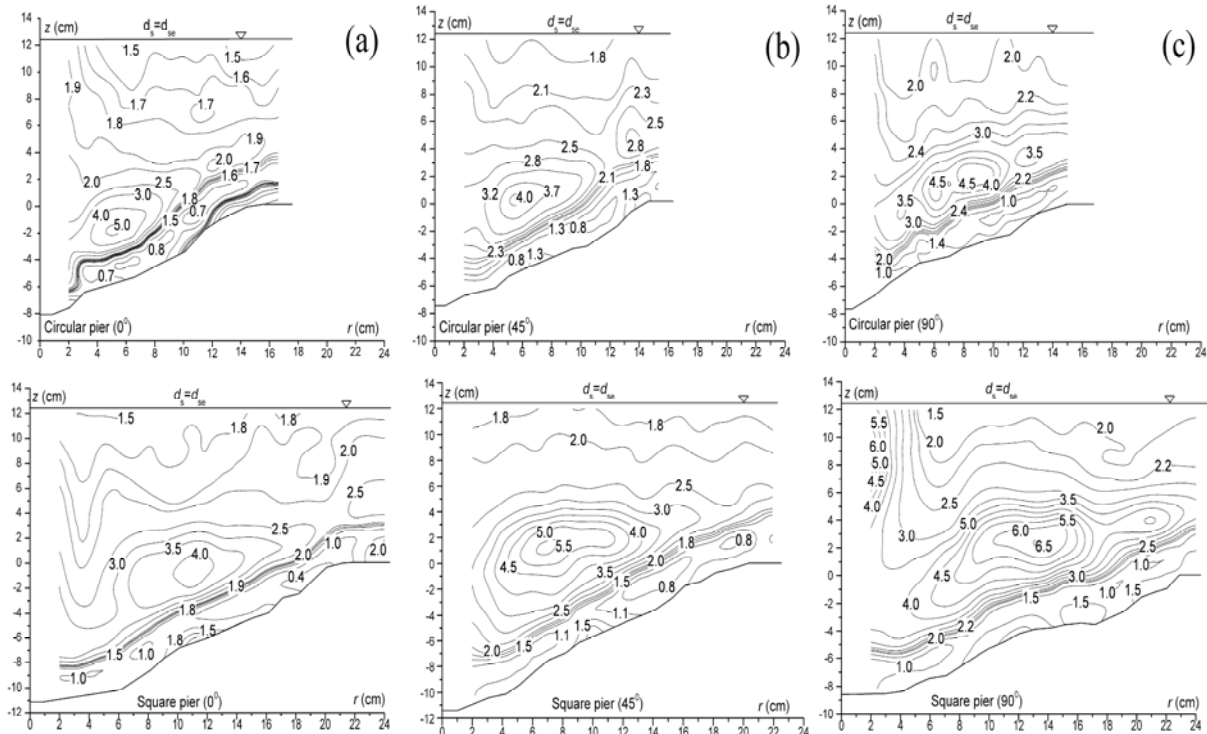


Fig. 10: Contours of tangential turbulence intensity u^+ (in cm/s) at azimuthal planes (a) $\theta = 0^\circ$, (b) $\theta = 45^\circ$ and (c) $\theta = 90^\circ$

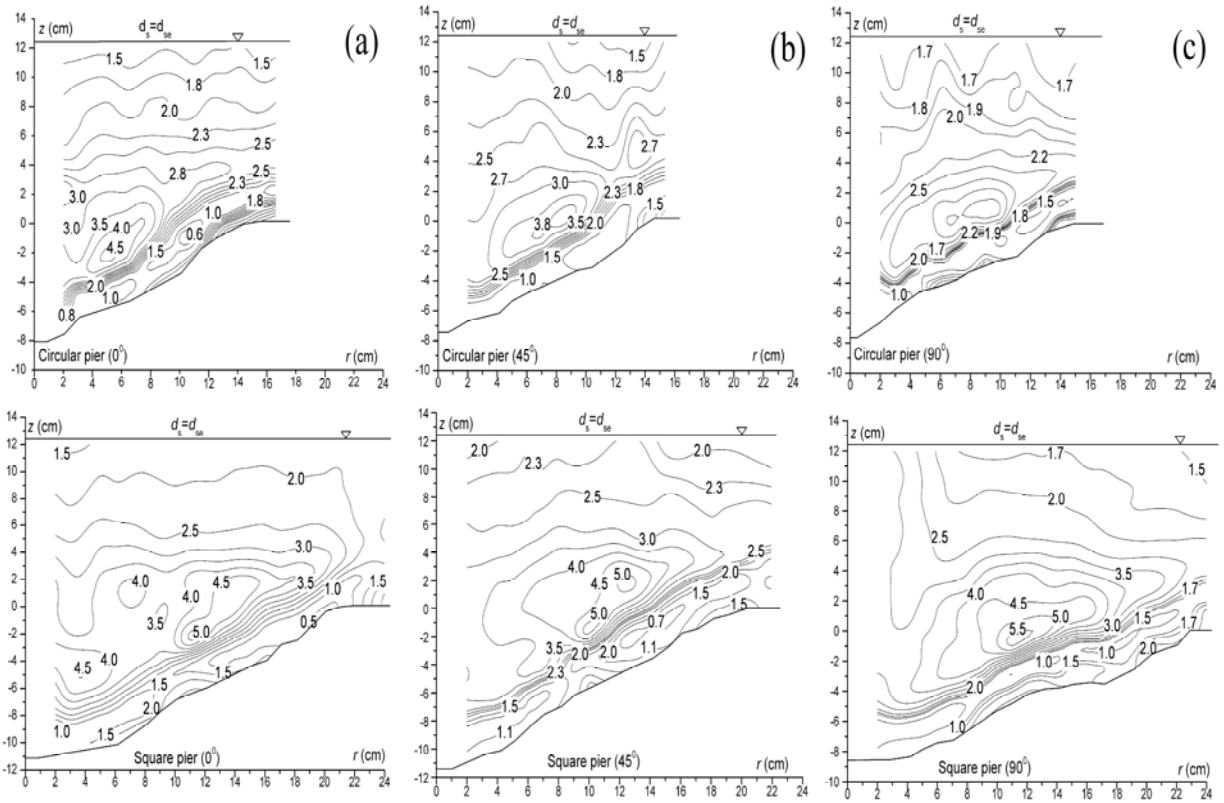


Fig 11: Contours of radial turbulence intensity v^+ (in cm/s) at azimuthal planes (a) $\theta = 0^\circ$, (b) $\theta = 45^\circ$ and (c) $\theta = 90^\circ$

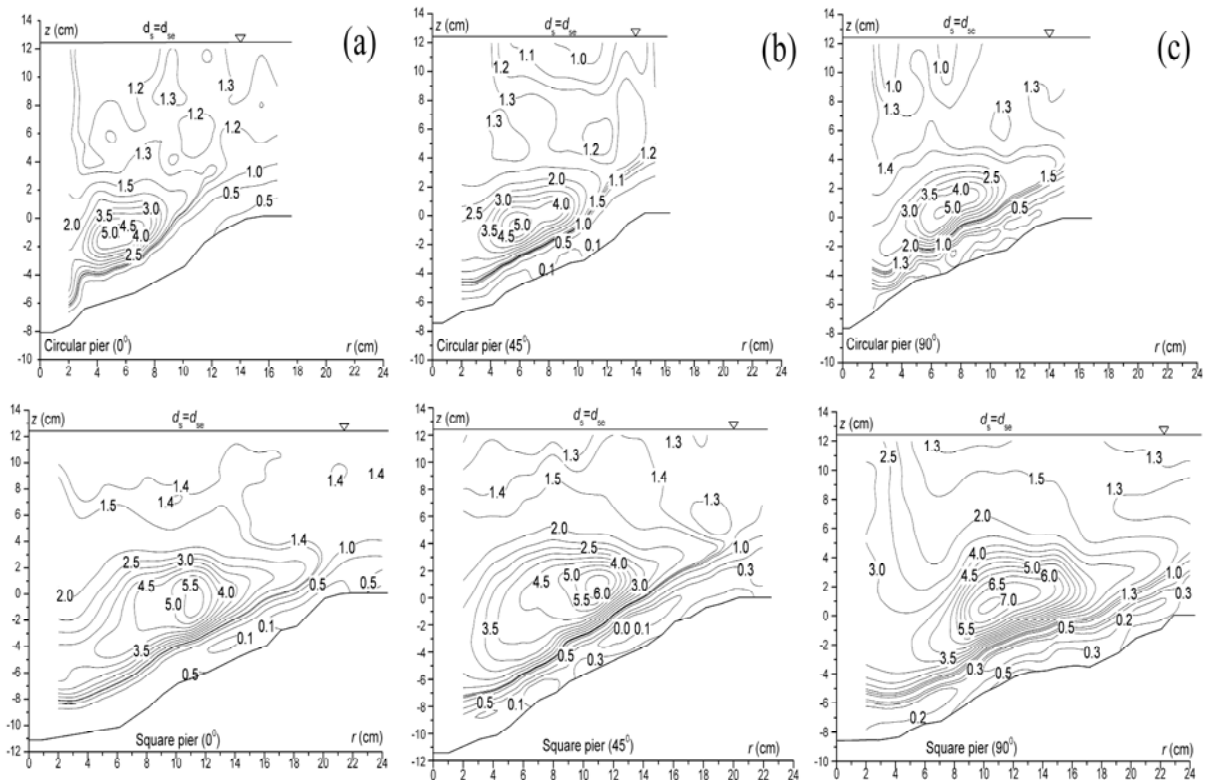


Fig. 12: Contours of vertical turbulence intensity w^+ (in cm/s) at azimuthal planes (a) $\theta = 0^\circ$, (b) $\theta = 45^\circ$ and (c) $\theta = 90^\circ$

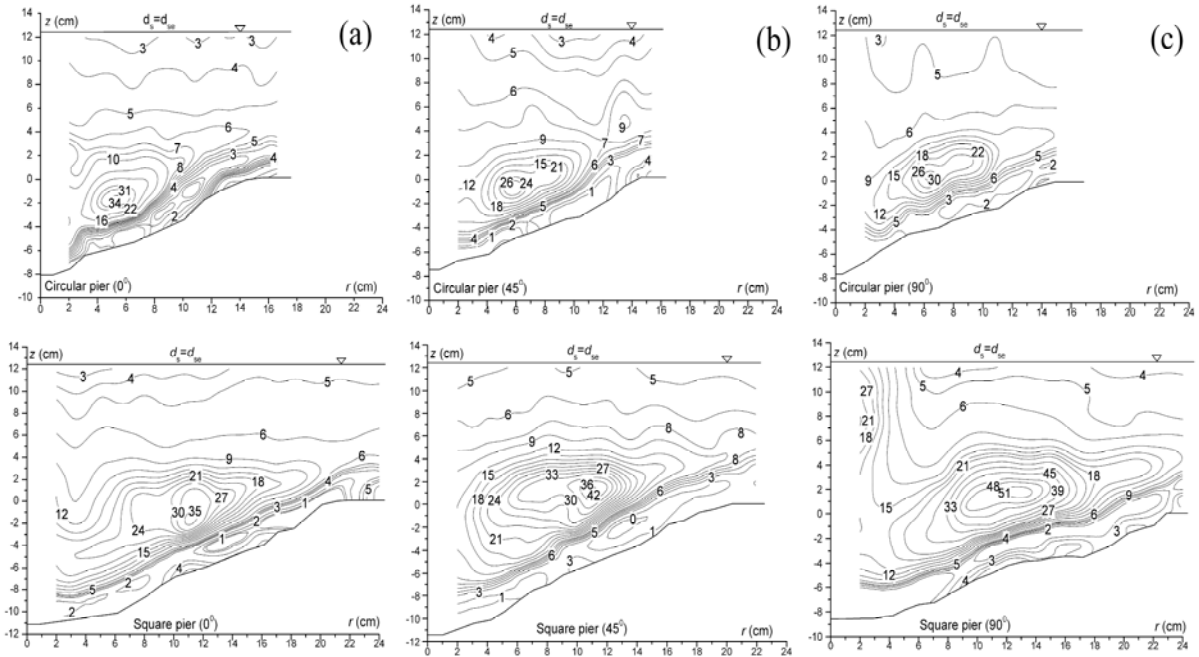


Fig. 13: Contours of turbulent kinetic energy k (in cm^2/s^2) at azimuthal planes (a) $\theta = 0^\circ$, (b) $\theta = 45^\circ$ and (c) $\theta = 90^\circ$

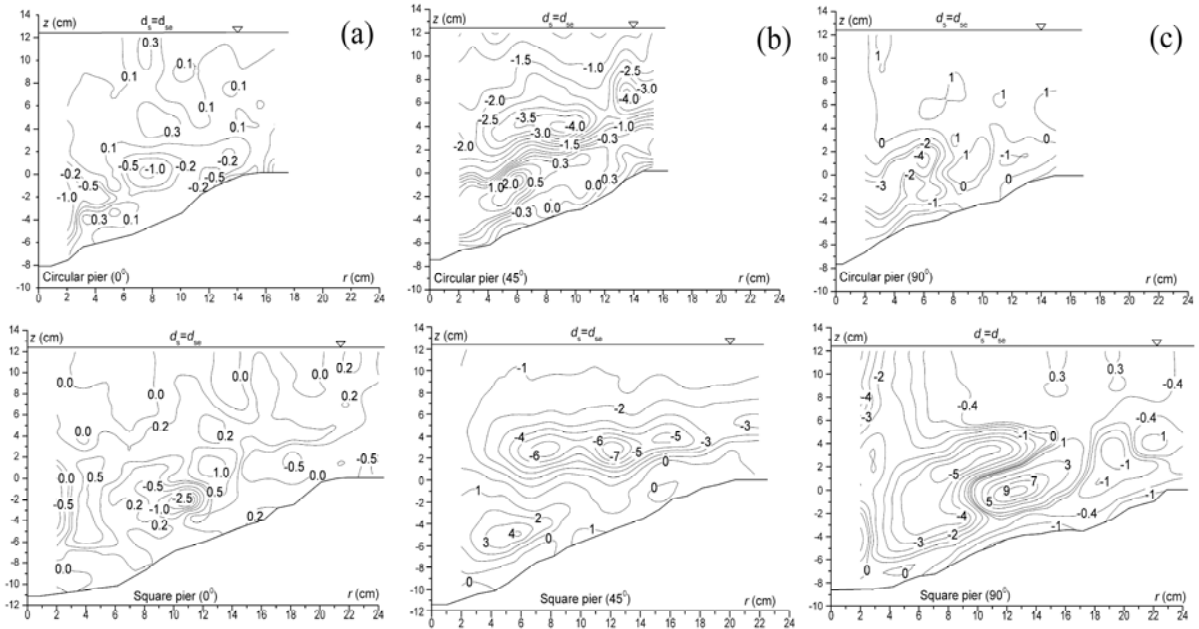


Fig. 14: Contours of $-\overline{u'v'}$ ($= \tau_{uv} / \rho$, in cm^2/s^2) at azimuthal planes (a) $\theta = 0^\circ$, (b) $\theta = 45^\circ$ and (c) $\theta = 90^\circ$

Figure 14a to c, 15a to c and 16a to c represent the contours of the Reynolds stresses $\tau_{uv} [= -\rho (\overline{u'v'})$, where ρ is the mass density of water], $\tau_{vw} [= -\rho (\overline{v'w'})$ and $\tau_{wu} [= -\rho (\overline{w'u'})$ at different azimuthal planes (0° , 45° and 90°) for equilibrium scour hole, respectively. In the plots, the Reynolds stresses are shown relative to the mass density ρ of water. The contours of τ_{uv} ,

changes sign from negative above the scour hole to positive inside the scour hole while the contours of τ_{vw} and τ_{wu} change from positive above the scour hole to negative inside the scour hole. There is a slight variation of the Reynolds stresses τ_{vw} and τ_{wu} above the scour hole, while they increase significantly inside the scour hole owing to the turbulent mixing of fluid as a result of the vertical flow. Therefore, a core

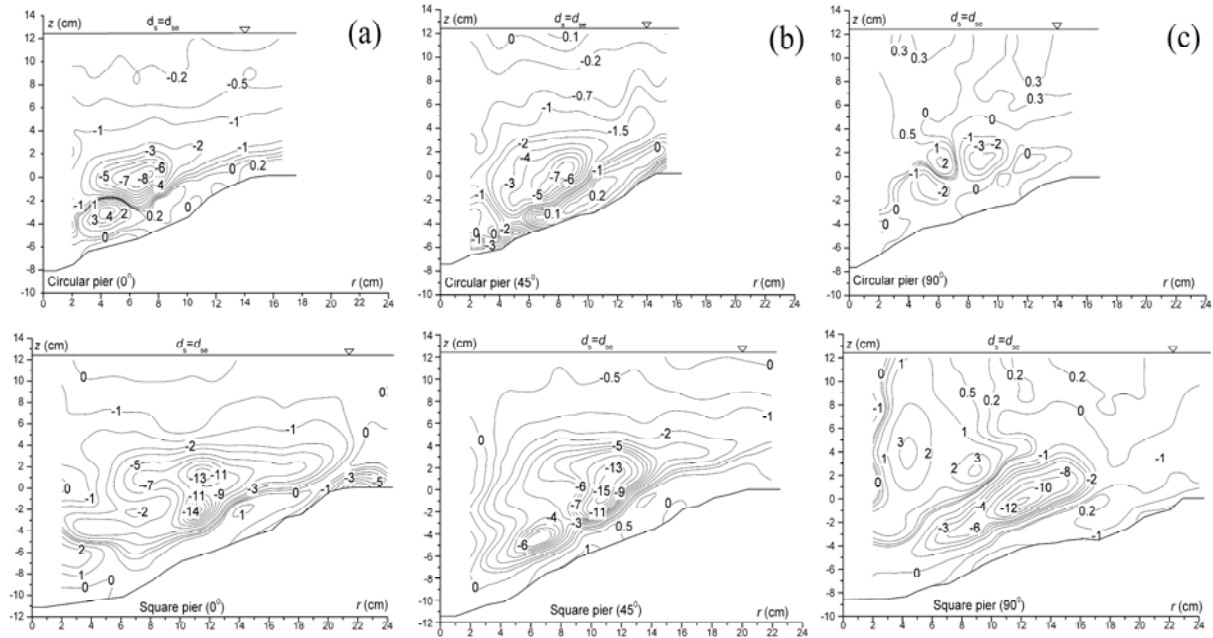


Fig. 15: Contours of $-\overline{v'w'}$ ($=\tau_{vw}/\rho$, in cm^2/s^2) at azimuthal planes (a) $\theta = 0^\circ$, (b) $\theta = 45^\circ$ and (c) $\theta = 90^\circ$

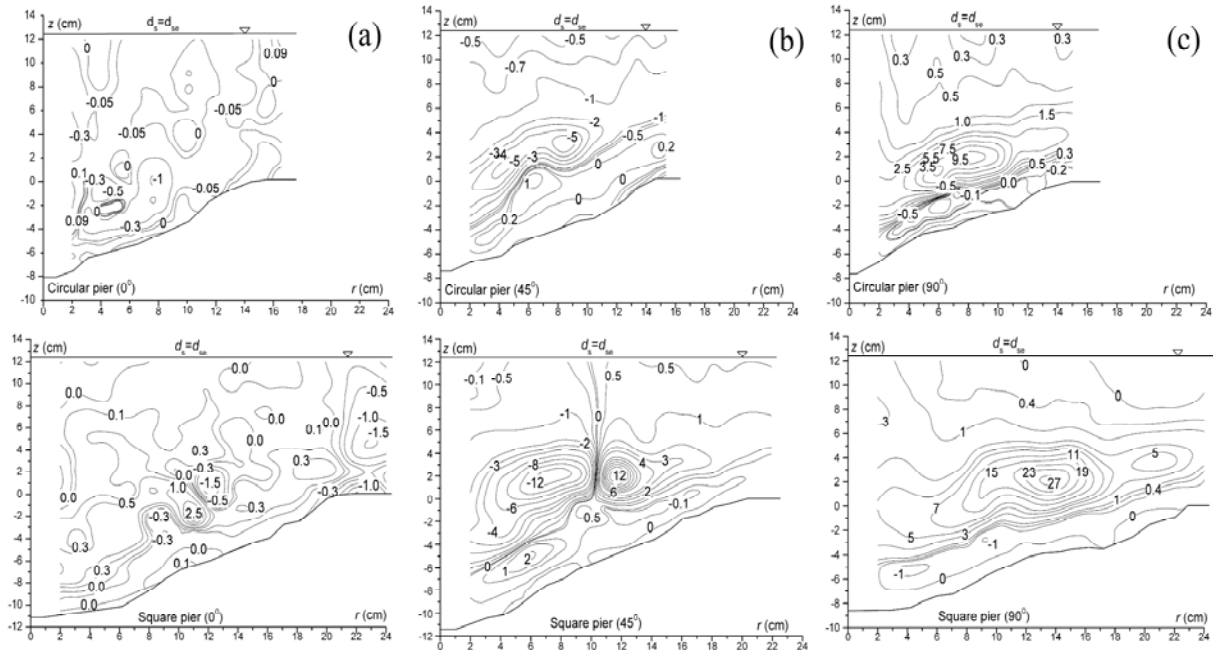


Fig. 16: Contours of $-\overline{w'u'}$ ($=\tau_{wu}/\rho$, in cm^2/s^2) at azimuthal planes (a) $\theta = 0^\circ$, (b) $\theta = 45^\circ$ and (c) $\theta = 90^\circ$

of higher magnitudes of τ_{vw} and τ_{wu} occurs at the central portion of the scour hole. But, close to the scoured bed, τ_{vw} and τ_{wu} reduce due to the lower magnitude (smooth flow) of upward velocity along the inclined bed of the scour hole. In general, inside the scour hole, the Reynolds stresses at 45° are higher than those at 0° and 90° .

Bed-shear stress: The bed-shear stress τ_b (time-averaged) acting within the scour hole is estimated using the distributions of the Reynolds stresses, as was done by Dey and Barbhuiya (2005), as follows:

$$\tau_b = \sqrt{\tau_\theta^2 + (\tau_r \cos \beta + \tau_z \sin \beta)^2} \Big|_{\text{at scoured bed}}$$

where,

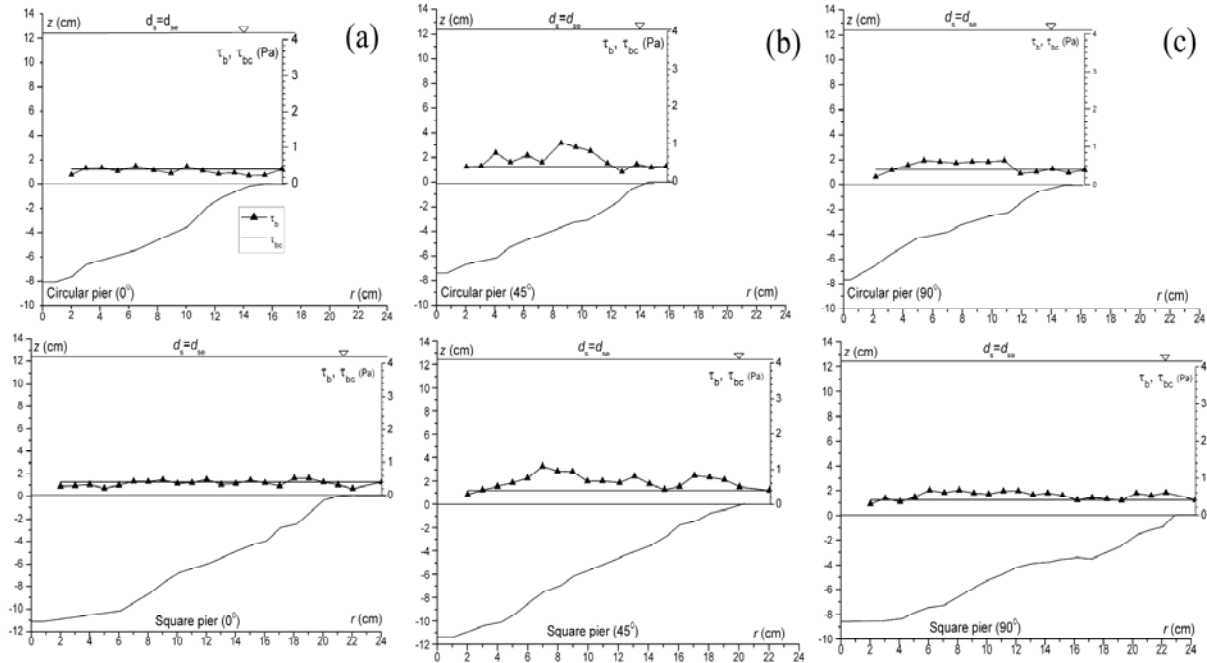


Fig. 17: Distributions of τ_b and τ_{bc} (in Pa) at azimuthal planes (a) $\theta = 0^\circ$, (b) $\theta = 45^\circ$ and (c) $\theta = 90^\circ$

$$\tau_\theta = \tau_{wu} + \tau_{uv}; \tau_r = \tau_{uv} + \tau_{vw}; \tau_z = \tau_{wu} + \tau_{vw};$$

and β is the local angle of the scoured bed with the horizontal. Figure 17a to c illustrates the variations of bed-shear stress τ_b with radial distance r_0 at different azimuthal planes for equilibrium scour holes at circular and square piers.

The bed-shear stress τ_b increases with increase in θ becoming maximum at 45° and then it decreases. It is in conformity with the results of Melville (1975), Dey and Bose (1994) and Dey and Raikar (2007). The bed shear stress τ_b also increases with increase in radial distance from the pier becoming maximum in the middle portion of the scour hole and then it decreases to take the value of τ_b on the flat bed.

The critical bed-shear stresses τ_{bc} (time-averaged) on the sloping bed, estimated using the method proposed by Dey (2003) for adverse sloping beds with oblique near-bed flow, are also plotted along with τ_b for the purpose of comparisons. To estimate τ_{bc} using the method proposed by Dey (2003), one requires information on critical bed-shear stress τ_c on a horizontal bed that was determined from the Shields diagram. In equilibrium scour holes, the values of τ_b are in general either almost equal or lower than τ_{bc} suggesting the equilibrium of scour. But at 45° and 90° ,

the higher values of τ_b than τ_{bc} indicate the effects of adverse slope and oblique near-bed flow. Melville (1975) and Dey and Raikar (2007) also had similar observations. Importantly, Dey (2003) identified that there exists an inconsistency between the experimental and estimated critical bed-shear stress on adverse sloping beds. This is the probable reason that τ_b values in some locations remain greater than τ_{bc} values. However, in case of a square pier, the magnitudes of τ_b are greater than those for a circular pier in an equilibrium scour hole.

COMPARISON OF THE CHARACTERISTICS OF HORSESHOE VORTEX

It is important to compare the present findings of the characteristics of horseshoe vortex at a square and circular pier which was also studied by Dey and Raikar (2007). The comparisons of the present findings are as follows:

- The magnitudes of u at a circular pier are greater than that at the corresponding locations of the flow zone at a square pier, as the size of the scour hole at a circular pier is smaller than that at a square pier
- The magnitudes of v at a circular pier are approximately 20-30% lower than that at the corresponding locations of the flow zone at a square pier
- The magnitude of downflow at a circular pier is slightly lower than that at the corresponding

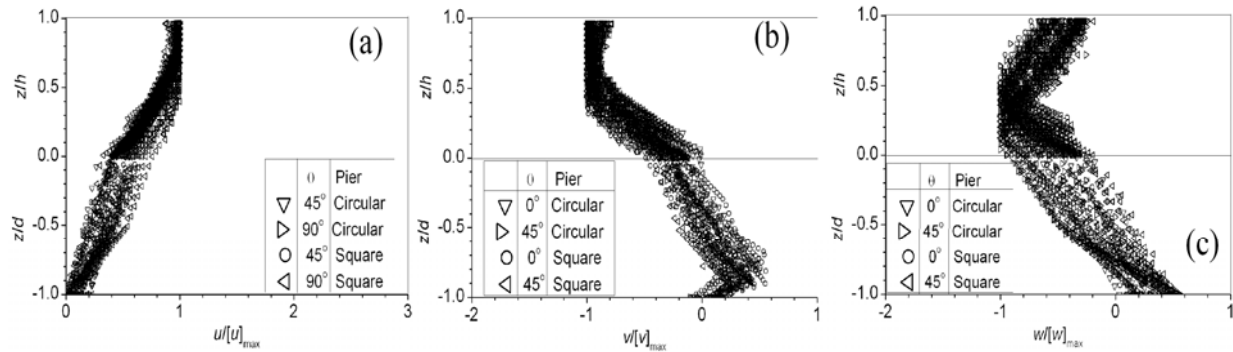


Fig. 18: Similarities of (a) u profiles, (b) v profiles and (c) w profiles

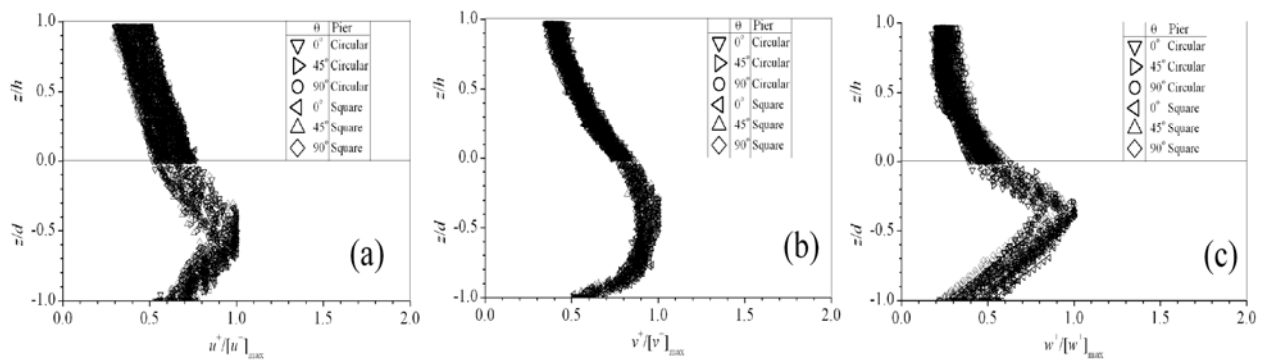


Fig. 19: Similarities of (a) u^+ profiles, (b) v^+ profiles and (c) w^+ profiles

locations of the flowzone at a square pier by approximately 10%

- In case of a circular pier, the size of the horseshoe vortex core is smaller than that of square pier
- The vorticity ω at a circular pier is approximately 30-40% weaker than that at a square pier
- The magnitude of circulation Γ for circular pier is 40-50% lower than the square pier
- In case of a circular pier, the turbulence intensities and the Reynolds stresses are lower than those for a square pier.

All the above findings are in satisfactory agreement with the results of Dey and Raikar (2007).

SIMILARITY OF VELOCITY AND TURBULENCE PROFILES

Two length scales d and h are introduced for the flow zone inside ($z \leq 0$) and above ($z > 0$) the scour hole, respectively, in order to group all the flow data together in horseshoe vortex flow at circular pier and square pier. Here, d is the local depth of the scour hole measured from the original bed level. The scales of the velocities u , v and w are considered as $[u]_{\max}$, $[v]_{\max}$ and $[w]_{\max}$ for the individual profiles, respectively. For v - and w -profiles, the data at $\theta = 90^\circ$ are not accounted, as the vortex flow is not prominent at $\theta = 90^\circ$. Then again,

for u -profile, the data at $\theta = 0^\circ$ are not included because the magnitude of u is negligible. Figure 18a to c show that all the flow data falls down of on a single band by using the proposed length and velocity scales. An emphasis is given for w -profiles on the downflow at the pier upstream. In case of turbulence intensities, consideration of the corresponding maximum turbulence intensity for the individual profiles makes possible to bring down all the data approximately on a single band. Figure 19a to c reveal some degree of collapse of the data plots of turbulence intensities, though the plots have considerable scatter. However, it is not possible to collapse the Reynolds stresses (tangential stress) data on a single band. The plausible reasons are due to a thorough mixing of fluid as a result of the vortex flow and hence the Reynolds stresses that are very sensitive to the turbulent fluctuations subject to uncertain decrease.

APPLICATIONS

The characteristics of horseshoe vortex that is considered to be the prime cause of scour at a circular and square pier are revealed from Fig. 4 to 13. In addition, Table 1 shows the information on the circulation that is believed to be the strength of the horseshoe vortex. In addition, the turbulence characteristics have significant role towards the

mobility of sediment particles inside the scour hole. Therefore, the present findings have immense importance in developing a mathematical model of local scour process at a circular and square pier including the influence of turbulence.

CONCLUSION

Clear water scour tests have been carried out on a circular and a square pier to measure the turbulent horseshoe vortex flow in an equilibrium scour hole by an acoustic Doppler velocimeter. The contours of time-averaged velocities, turbulence intensities and Reynolds stresses at different azimuthal planes for the equilibrium scour holes have been presented. The velocity is reversal inside the scour hole forming a horseshoe vortex. The maximum downflow at pier upstream measured was 0.7 times the average approaching flow velocity at $\theta = 0^\circ$ and $z = -0.021$ m. The vector plots of the flow field present a good understanding of the change of the horseshoe vortex in an equilibrium scour hole. The horseshoe vortex is a forced vortex. The size of the horseshoe vortex core (having the shape of an ellipse) being confined to inside the scour hole is more prominent in case of square pier compared to circular pier. The circulations of horseshoe vortex have been worked out from the vorticity contours by using the Stokes theorem.

The circulations decrease with an increase in azimuthal angle. A core of higher magnitude of turbulence intensities and Reynolds stresses exists inside the scour hole. The characteristics of horseshoe vortex flow have been investigated from the viewpoint of similarity proposing the plausible velocity and turbulence characteristic scales. Interestingly, both the flow and turbulence intensities in horseshoe vortex flow in an equilibrium scour hole are found to be probably similar.

NOTATION

The following symbols were used in this study:

A	=	Area enclosed between successive vorticity contours [L^2]
b	=	Pier width [L]
d_s	=	Scour depth measured at any instant from initial bed level [L]
d_{se}	=	Equilibrium scour depth [L]
d_{16}	=	16% finer sand diameter [L]
d_{50}	=	Median diameter of sand [L]
d_{84}	=	84% finer sand diameter [L]
\overline{ds}	=	Differential displacement vector over a closed curve

F_r	=	Froude number of flow [—]
F_t	=	$\left(\frac{U}{u_c}\right)$ Threshold Froude number [—]
g	=	Gravitational acceleration [LT^{-2}]
h	=	Approaching flow depth [L];
h/b	=	Non-dimensional inflow depth [—]
i, k	=	Direction indices along r and z axis respectively [—]
k	=	$[0.5(u'^2+v'^2+w'^2)]$ Turbulent kinetic energy [L^2T^{-2}]
Q	=	Discharge [$L^3 T^{-1}$]
r	=	Radial distance [L]
R_e	=	$\left(\frac{Uh}{\nu}\right)$ Flow Reynolds number [—]
R_p	=	$\left(\frac{Ub}{\nu}\right)$ Pier Reynolds number [—]
s	=	$\left(\frac{\rho_s}{\rho}\right)$ Relative density of sand [—]
U	=	Depth-averaged approaching flow velocity [LT^{-1}]
u	=	Time-averaged tangential velocity [LT^{-1}]
u_c	=	Critical velocity [LT^{-1}]
u'	=	Fluctuation of u [LT^{-1}]
u^+	=	$\left(\overline{u'u'}\right)^{0.5}$ [LT^{-1}]
v	=	Time-averaged radial velocity [LT^{-1}]
V	=	$\left(\sqrt{u^2 + v^2 + w^2}\right)$ Time-averaged absolute velocity [LT^{-1}]
\mathbf{V}	=	$\left(\sqrt{v^2 + w^2}\right)$ Time-averaged velocity vector [LT^{-1}]
\overline{V}	=	Velocity vector over a closed curve
v'	=	Fluctuation of v [LT^{-1}]
v^+	=	$\left(\overline{v'v'}\right)^{0.5}$ [LT^{-1}]
w	=	Time-averaged velocity in the z -direction [LT^{-1}]
w'	=	Fluctuation of w [LT^{-1}]
w^+	=	$\left(\overline{w'w'}\right)^{0.5}$ [LT^{-1}]
z	=	Vertical distance [L]
ρ	=	Mass density of water [ML^{-3}]
ρ_s	=	Mass density of sand [ML^{-3}]
Γ	=	Circulation [L^2T^{-1}]
τ_b	=	Local bed-shear stress in scour hole [$ML^{-1}T^{-2}$]

τ_{bc}	=	Critical bed-shear stress on adverse sloping beds with oblique near-bed flow [ML ⁻¹ T ⁻²]
τ_c	=	Critical bed shear stress on horizontal bed [ML ⁻¹ T ⁻²]
τ_r	=	Radial bed-shear stress [ML ⁻¹ T ⁻²]
τ_z	=	Vertical bed-shear stress [ML ⁻¹ T ⁻²]
τ_θ	=	Tangential bed-shear stress [ML ⁻¹ T ⁻²]
σ_g	=	Geometric standard deviation [—]
θ	=	Azimuthal angle [—]
β	=	Local angle of scoured bed with horizontal [—]
ϕ	=	Angle of repose [—]
ω	=	Vorticity [T ⁻¹]
ν	=	Kinematic viscosity [L ² T ⁻¹]

ACKNOWLEDGMENT

This investigation is a part of doctoral dissertation work by the first author in the School of Water Resources Engineering, Jadavpur University, Kolkata, India under the supervision of Prof. (Dr.) Asis Mazumdar, Director of the School. The helpful suggestions from Prof. (Dr.) Subhasish Dey, Brahma Putra Chair Professor for Water Resources, Department of Civil Engineering, Indian Institute of Technology Kharagpur, India is gratefully acknowledged.

REFERENCES

- Abed, L. and M.M. Gasser, 1993. Model study of local scour downstream bridge piers. Proceeding of National Conference Hydraulic Engineering. San Francisco, pp: 1738-1743.
- Ahmed, F. and N. Rajaratnam, 1998. Flow around bridge piers. *J. Hydraul. Eng.*, 124(3): 288-300.
- Barbhuiya, A.K. and S. Dey, 2004. Local scour at abutments: A review. *Acad. Sci.*, 29(October): 449-476.
- Breusers, H.N.C., G. Nicollet and H.W. Shen, 1977. Local scour around cylindrical piers. *J. Hydraul. Res.*, 15(3): 211-252.
- Dey, S., 1995. Three-dimensional vortex flow field around a circular cylinder in a quasi-equilibrium scour hole. *Sadhana, Proc. Indian Acad. Sci.*, 20: 871-885.
- Dey, S., 2003. Threshold of sediment motion on combined transverse and longitudinal sloping beds. *J. Hydraul. Res.*, 41(4): 405-415.
- Dey, S. and A.K. Barbhuiya, 2005. Turbulent flow field in a scour hole at a semicircular abutment. *Can. J. Civ. Eng.*, 32(1): 213-232.
- Dey, S. and R.V. Raikar, 2007. Characteristics of horseshoe vortex in developing scour holes at piers. *J. Hydraul. Eng. ASCE*, 133(4): 399-413.
- Dey, S. and S.K. Bose, 1994. Bed shear in equilibrium scour around a circular cylinder embedded in loose bed. *Appl. Math. Model.*, 18(5): 265-273.
- Dey, S., S.K. Bose and G.L.N. Sastry, 1995. Clear water scour at circular piers. *J. Hydraul. Eng. ASCE*, 121(12): 869-876.
- Froehlich, D.C., 1989. Local scour at bridge abutments. *Proceeding of National Conference on Hydraulic Engineering*. New York, pp: 13-18.
- Graf, W.H. and I. Istiarto, 2002. Flow pattern in the scour hole around a cylinder. *J. Hydraul. Res.*, 40(1): 13-20.
- Istiarto, I. and W.H. Graf, 2001. Experiments on flow around a cylinder in a scoured channel bed. *J. Sediment Res.*, 16(4): 431-444.
- Jain, S.C. and E.E. Fischer, 1979. Scour around bridge piers at high Froude numbers. Report No. FHWA-RD-79-104, Federal Highway Administration, Washington, D.C.
- Khawairakpam, P., S.S. Ray, S. Das, R. Das and A. Mazumdar, 2012. Scour hole characteristics around a vertical pier under clear water scour conditions. *ARPN J. Eng. Appl. Sci.*, 7(6): 649-654.
- Laursen, E.M. and A. Toch, 1956. Scour around bridge piers and abutments. *Bull. No. 4*, Iowa Highway Research Board, Ames, Iowa.
- Liu, H. K., F.M. Chang and M.M. Skinner, 1961. Effect of bridge constriction on scour and backwater, Report No. CER60HKL22, Civil Eng. Sect., Colorado State Univ., Fort Collins, Colo.
- Melville, B.W., 1975. Local scour at bridge sites. Report No. 117, School of Eng., Univ., of Auckland, New Zealand.
- Melville, B.W., 1992. Local scour at bridge abutments. *J. Hydraul. Eng. ASCE*, 118(4): 615-631.
- Muzzammil, M. and T. Gangadhariah, 2003. The mean characteristics of horseshoe vortex at a cylindrical pier. *J. Hydraul. Res.*, 41(3): 285-297.
- Oliveto, G. and W.H. Hager, 2002. Temporal evolution of clear-water pier and abutment scour. *J. Hydraul. Eng. ASCE*, 128(9): 811-820.
- Raudkivi, A.J. and R. Ettema, 1983. Clear-water scour at cylindrical piers. *J. Hydraul. Eng. ASCE*, 109(3): 338-350.
- Richardson, J.R. and E.V. Richardson, 1994. Practical method for scour prediction at bridge piers. *Proceeding of ASCE National Conference on Hydraulic Engineering*. Buffalo, NY, pp: 1-5.
- Shen, H.W., V.R. Schneider and S. Karaki, 1969. Local scour around bridge piers. *J. Hydraul. Div. ASCE*, 95(HY6): 1919-1940.